JGR Atmospheres

RESEARCH ARTICLE
10.1029/2021JD035969

The Control of Plant and Soil Hydraulics on the Interannual Variability of Plant Carbon Uptake Over the Central US

Xue-Yan Zhang[1], Guo-Yue Niu[1], and Xubin Zeng[1]

[1]Department of Hydrology and Atmospheric Sciences, The University of Arizona, Tucson, AZ, USA

Key Points:

- Observation-based estimates of annual gross primary productivity (GPP) show a strong dependence on water availability over the central US
- A land surface model with adequate representations of plant and soil hydraulics can capture the observed interannual variability of GPP
- A model with a low plant drought resilience substantially overestimates GPP sensitivity to water availability

Supporting Information:

Supporting Information may be found in the online version of this article.

Correspondence to:

G.-Y. Niu,
niug@email.arizona.edu

Citation:

Zhang, X.-Y., Niu, G.-Y., & Zeng, X. (2022). The control of plant and soil hydraulics on the interannual variability of plant carbon uptake over the central US. *Journal of Geophysical Research: Atmospheres*, *127*, e2021JD035969. https://doi.org/10.1029/2021JD035969

Received 6 OCT 2021
Accepted 18 APR 2022

Author Contributions:

Conceptualization: Guo-Yue Niu
Data curation: Xue-Yan Zhang
Formal analysis: Xue-Yan Zhang
Funding acquisition: Guo-Yue Niu, Xubin Zeng
Methodology: Xue-Yan Zhang
Project Administration: Xubin Zeng
Software: Xue-Yan Zhang
Supervision: Guo-Yue Niu
Validation: Xue-Yan Zhang
Visualization: Xue-Yan Zhang
Writing – original draft: Xue-Yan Zhang
Writing – review & editing: Guo-Yue Niu, Xubin Zeng

Abstract The interannual variability (IAV) of gross primary productivity (GPP) reflects the sensitivity of GPP to climate variations and contributes substantially to the variations and long-term trend of the atmospheric CO_2 growth rate. Analyses of three observation-based GPP products indicate that their IAVs are consistently correlated to terrestrial water storage anomaly over the central US, where episodic droughts occur. A land surface model explicitly representing plant hydraulics and groundwater capillary rise with an adequate soil hydraulics well captures the observed GPP IAV. Our sensitivity experiments indicate that, without representations of plant hydraulics and groundwater capillary rise or using an alternative soil hydraulics, the land model substantially overestimates the GPP IAV and the GPP sensitivity to water in the central US. This study strongly suggests the use of the van Genuchten water retention model to replace the most commonly used Brooks–Corey model, which generally produces too strong matric suction of soil water especially in dry conditions, in land surface modeling. This study highlights the importance of plant and soil hydraulics and surface–groundwater interactions to Earth system modeling for projections of future climates that may experience more intense and frequent droughts.

Plain Language Summary The interannual variability (IAV) of land carbon uptake contributes substantially to the fluctuations of atmospheric CO_2 growth rate. Consistent with previous studies, our data analyses of various observation-based gross primary productivity (GPP) products and land water storage change data reveal a positive GPP–water relationship. This relationship also has been used to evaluate and constrain climate model projections. Our model sensitivity experiments suggest that current land surface models may overestimate the GPP–water sensitivity and potentially degrade the credibility of future climate projections, due to a lack of appropriate plant and soil hydraulics and surface–groundwater interactions. Our results highlight the importance of key ecohydrological processes on IAV of GPP as well as CO_2 projections.

1. Introduction

Global terrestrial ecosystems have served as a substantial sink of the atmospheric CO_2, offsetting about one third of the world's fossil fuel emissions and thereby slowing the rise of atmospheric CO_2 concentration (Quéré et al., 2018; Wolf et al., 2016). As the largest terrestrial carbon fluxes, gross primary productivity (GPP) dominates the net land carbon sink (or net ecosystem exchange; NEE) and hence the land carbon storage; its interannual variability (IAV) contributes the most to the IAV in NEE and that of the atmospheric CO_2 concentration (Bousquet et al., 2000). The GPP IAV also contributes substantially to the long-term trend in GPP due to asymmetric responses of GPP to dry and wet conditions (Green et al., 2019). Moreover, the relationships between the NEE IAV and the IAVs in air temperature and water availability has been used to quantify the sensitivities of the land carbon storage to air temperature and water availability (Cox et al., 2013; Humphrey et al., 2018; Jung et al., 2017) and served as a constraint on Earth System Models (ESMs; Cox et al., 2013).

GPP is very sensitive to drought stress, especially in the water-limited, semiarid regions through reduced stomatal conductance and its impact on CO_2 diffusion (Lin et al., 2015) as well as dehydration effect on metabolic capacity and plant morphology (Sun et al., 2020). Poulter et al. (2014) attributes the 2011 record high global carbon uptake to the responses of the semiarid ecosystems in Australia to an anomalous wet period associated with El Niño–Southern Oscillation. Ahlström et al. (2015) suggested that precipitation, associated with ENSO, is even a stronger driver than temperature for the GPP IAV in semiarid regions, with negative GPP anomalies being associated with warm and dry climates and positive GPP anomalies with cool and wet climates. An analysis of flux tower data at 25 sites in the southwest North America semiarid ecosystems further confirms the high sensitivity of GPP to precipitation variations (Biederman et al., 2017). Recent studies highlight the dominance of water

availability on the net land carbon uptake (Humphrey et al., 2018, 2021). Humphrey et al. (2018) suggested that terrestrial water storage anomaly (TWSA), rather than the temperature anomaly, is more strongly related to the IAV of the net carbon sink at either local or global scale. Green et al. (2019) also found that the nonlinear GPP responses to soil moisture variability can lead to intensified reductions in the land carbon sinks. *These observation-based analyses inspire us to evaluate models' representations of GPP dependence on water availability and thus to discern the dominant mechanisms controlling the modeled GPP IAV with a focus on the modeled ecosystem response to droughts.*

The responses of plant carbon uptake to drought stresses are not fully understood or represented in current ESMs. Most land surface models (LSMs) for use in ESMs predict low plant drought resilience as reflected by the negative biases in the modeled rainfall use efficiency (RUE; Ma et al., 2017; Zhu et al., 2019). This model deficiency may substantially contribute to the uncertainties in the land carbon sink and atmospheric CO_2 concentration projected by ESMs with regard to the uncertainty in the water sensitivity of GPP in addition to that in the temperature uncertainty (Arora et al., 2020; Friedlingstein et al., 2006). Moreover, the Brooks–Corey (Brooks & Corey, 1964) or Clapp–Hornberger (CH; Clapp & Hornberger, 1978) soil water retention model is most commonly used in LSMs and overestimates the soil matrix suction head, resulting in low root water uptakes and GPP, especially at low soil water conditions (Niu et al., 2020). Current ESMs indicate that soil moisture variability contributes to 90% of IAV of global land carbon uptake mainly through photosynthesis (Humphrey et al., 2021). *However, we argue that current ESMs may significantly overestimate the water sensitivity of GPP due to inadequate representations of key ecohydrological controls.*

Plant and soil hydraulics are known to strongly regulate and even attenuate the impacts of atmospheric and soil water stress on vegetation productivity (Y. Liu et al., 2020). Previous studies have observed various vegetation water use strategies for maintaining stomata opening and thus photosynthesis rates during dry seasons through increasing rooting depth (Zhou et al., 2020), optimizing vertical root distribution (Fan et al., 2017), redistributing soil water by roots (Bleby et al., 2010; J.-E. Lee et al., 2005), allocating more photosynthetic production to roots, and storing excessive wet-season water in the plant stem (Loustau et al., 1998), etc. Wang et al. (2018) reported that phreatophytes under a hyperarid climate can consume water (~10 times of precipitation) primarily through deep roots extracting water from the capillary fringe and groundwater. J.-E. Lee et al. (2005) estimated transpiration in the Amazonia during dry seasons can be increased by 40% with hydraulic redistribution (HR) based on global circulation modeling. Moreover, soil water potential determined by soil texture and soil water content directly influences root water uptake rate and HR. Therefore, plant and soil hydraulics can allow vegetation to maintain stomatal openings and vegetation carbon uptake during dry periods.

In this study, we first analyzed the relationships between the IAV of various GPP products and Gravity Recovery and Climate Experiment (GRACE) terrestrial water storage (TWS) anomaly data and obtained an observation-based water sensitivity of GPP, similarly to the analyses of Humphrey et al. (2018) but with a focus on the central US. We selected the conterminous US domain (CONUS) due to data availability and accuracy. The central US is a dry-to-wet transition region, experiencing the most intense episodic droughts. Also, it is a "hot-spot" of strongest land–atmosphere coupling (Koster et al., 2004), implying that regional ecosystem response, in terms of strength and timing ("memory"), to climate variability may feedback to affect climate variability. Using the observation-based water sensitivity of GPP, we then assessed LSMs with different representations of plant water stress to understand the dominant ecohydrological processes that may control the water sensitivity of GPP. We used a recent version of the Noah-MP LSM (Niu et al., 2011) with explicit representations of groundwater capillary rise (Niu et al., 2007), plant hydraulics (Niu et al., 2020), and options of soil hydraulics. We aim to demonstrate the important roles of plant root water uptake, soil hydraulics, and groundwater capillary rise on plant photosynthesis over the central US and that a model lack of elaborate representations of these processes may significantly underestimate plant drought resilience and overestimate the water sensitivity of GPP. In this study, we used monthly RUE to measure plant drought resilience.

2. Methodology

2.1. Data

2.1.1. Reference Products of Vegetation Productivity and TWSA

To characterize uncertainty from observed GPP products, we used three GPP products derived from data-driven, satellite-based production efficiency, and statistical models, including the flux tower network (FLUXNET) model tree ensembles (MTEs), Moderate Imaging Spectroradiometer (MODIS), and Solar-induced chlorophyll fluorescence (SIF)-based product (GOSIF), respectively. The monthly 0.5° FLUXNET gridded data set is upscaled with in situ observations of water, carbon, and energy fluxes at FLUXNET eddy-covariance sites through MTE machine learning from 1982 to 2011 (Jung et al., 2011). The 8-day 1-km MODIS GPP product was generated using a simple light use efficiency model (MOD17A2), which relates GPP to photosynthetically active radiation absorbed by the vegetation canopy and is also adjusted by the vegetation-dependent radiation use conversion efficiency as well as water and temperature stresses (Zhao & Running, 2010; Zhao et al., 2005, 2006). The 8-day and 0.05° GOSIF GPP product is the ensemble mean of eight GPP products derived from the fine-scale global OCO-2-based SIF product (X. Li & Xiao, 2019a) with eight linear GPP–SIF relationships that includes four linear forms (universal and biome specific, with and without intercept) at site and grid-cell levels (X. Li & Xiao, 2019b). Global annual GPP estimated by this SIF-based GPP product exceeds that of the FLUXNET gridded data set and MODIS GPP (X. Li & Xiao, 2019b). Besides GPP products, we also used an MODIS leaf area index (LAI) product with a spatial resolution of 1 km and a temporal resolution of 8 days that has been significantly improved by reducing uncertainties from snow and cloud cover, instrument, and retrieval algorithm (Yuan et al., 2011). We reprocessed these GPP and MODIS LAI products into a spatial resolution of 0.125° and aggregated into yearly products for the period of 2001–2015 for MODIS and GOSIF products while 2001–2011 for the FLUXNET product due to the data availability.

Because precipitation is not enough to reflect the actual water availability for vegetation growth (Humphrey et al., 2018), we used the GRACE TWSA data to investigate the relationship between GPP and water availability. We adjusted three 1° monthly GRACE TWSA products with the gain factors to minimize the uncertainty related to their postprocessing processes and averaged these data sets during 2003–2015 to reduce their noises because of various resolutions (Landerer & Swenson, 2012; Sakumura et al., 2014). Because of the brevity of GRACE TWSA, we used a recently reconstructed TWSA product (F. Li, Kusche, et al., 2021) during 1982–2011 to examine the long-term GPP–TWSA relationship. We also evaluated modeled evapotranspiration (ET) and its components using a monthly 0.5° observation-driven Penman–Monteith–Leuning (PML) product because ET can significantly influence land surface water availability. This PML product has been comprehensively validated across site and global scales and widely used in exploring global ET changes (Y. Zhang et al., 2016). Here, we resampled this PML product into 0.125° through bilinear interpolation.

2.1.2. Forcing

In this study, we selected the hourly and 0.125° forcing data set of Phase 2 of the North American Land Data Assimilation System (NLDAS-2; Xia et al., 2012) to drive Noah-MP, including precipitation, downward shortwave and longwave radiation, surface air temperature and pressure, wind, and specific humidity. The global 1-km hybrid State Soil Geographic Database and the USGS 24-category vegetation data were resampled into a resolution of NLDAS-2 and then used to determine dominant soil and vegetation types at a grid-cell level in our modeling experiments.

2.2. Model and Experiments

The Noah-MP LSM is an improved version of the Noah LSM with multiple options of key physical processes to represent energy, water, and carbon flux exchanges between the land surface and the atmosphere (Niu et al., 2011; Yang et al., 2011). Noah-MP represents one canopy layer, up to three snow layers depending on the snow depth, four soil layers with a total depth of 2 m, and an unconfined aquifer. Noah-MP adopts the simple bucket-type groundwater model of Niu et al. (2007) to represent groundwater recharge into the aquifer (or "bucket") in wet periods and groundwater capillary rise from the "bucket" during dry periods. The explicit aquifer representation better captures TWSA than a deeper soil profile because it reduces the model dependence on subsurface hydrologic parameters, such as soil porosity and soil texture (Gulden et al., 2007). Noah-MP also introduces a

micropore volume fraction (f_{mic}; 0–1) to reduce groundwater capillary rise due to the presence of macropores associated with soil aggregates, plant roots, and worm holes (Beven & Germann, 1982). Noah-MP can represent a full groundwater capillary rise effect ($f_{mic} = 1$) and free drainage boundary condition at the soil bottom ($f_{mic} = 0$) by varying f_{mic}. The rate of gross photosynthesis (or GPP) is computed as the minimum of three limiting factors: Rubisco limitation, light limitation, and that associated with transport of photosynthetic products for C_3 plants and PEP-carboxylase limitation for C_4 plants (Bonan, 1996). It also includes a short-term vegetation phenology model that describes allocation of the assimilated carbon to various parts of the plant (root, leaf, stem, and wood), death due to cold and drought stresses, and turnover due to senescence, herbivory, or mechanical loss (Dickinson et al., 1998).

In this study, we used the recent version of Noah-MP with improved plant and soil hydraulics to enhance the modeled plant drought resilience (Niu et al., 2020). The new Noah-MP explicitly represents dynamic plant water storage supplied by root water uptake through hydrotropic root growth to meet transpiration needs, reflecting the tight coupling between water and carbon cycles. Noah-MP incorporates a macroscopic root water uptake model, which represents the lumped effects of vertical distribution in root surface area density on root water uptakes from each soil layer, Q_R, with a total depth of 2 m (more details in Niu et al., 2020):

$$Q_R = \sum_1^{N_R} Q_{R,i} = \sum_1^{N_R} A_{R,i} \frac{h_{s,i} - h_R}{\Omega_R + \Omega_{s,i}} \tag{1}$$

where i represents the ith root layer, N_R is the number of total soil layers containing roots (4 in this study for all vegetation types), $A_{R,i}$ is the root surface area per unit ground area (RAI; m^2/m^2), $h_{s,i}$ is the soil matrix suction head (m), h_R is the root suction head (m), Ω_R is the root radial resistance to water flow through roots (s), and $\Omega_{s,i}$ is the resistance for water flowing from ambient soil toward root surface in the ith layer (s). Q_R is the sum of root water uptake from all layers (m/s). Noah-MP assumes an equilibrium hydraulic state between all parts of plant (leaf, stem, and all root layers), and thus h_R is assumed to be close to the leaf water head. A observation-based relationship between leaf water head and relative water loss (Roderick & Canny, 2005) is used in this model to convert plant water storage to h_R. Plant absorbs soil water through roots (positive $Q_{R,i}$) and releases water to soil layers (negative $Q_{R,i}$), which represents HR through water exchanges between soils and roots at different depths. Moreover, Noah-MP represents the plant water availability (β) as a function of plant water storage, instead of soil water availability, to regulate transpiration and photosynthesis processes:

$$\beta = \max\left(0.0, \frac{M_q - M_{q,wilt}}{M_{q,max} - M_{q,wilt}}\right), \tag{2}$$

where M_q represents the plant water amount (mm), $M_{q,wilt}$ is the minimum plant water storage at a wilting point of 30 bar (mm), and $M_{q,max}$ is the maximum plant water storage (mm). It should be noted that M_q and $M_{q,max}$ refer to the whole plant water storage. $M_q - M_{q,wilt}$ is the available plant water storage for transpiration, while $M_{q,max} - M_{q,wilt}$ is the maximum plant water storage that can be used for transpiration. $M_{q,max}$ is converted from plant dry biomass using a vegetation-dependent ratio of the maximum plant water to dry biomass (Niu et al., 2020). This version also develops options of soil hydraulics by adding the van Genuchten (VG) water retention model (van Genuchten, 1980) in parallel with the original CH model (Clapp & Hornberger, 1978; Figure 1).

We conducted three experiments: (a) CTRL with all the new improvements including the plant hydraulics with dynamic roots (Niu et al., 2020), the VG soil water retention model, and groundwater capillary rise (Table S1 in Supporting Information S1); (b) LowR, based on CTRL, but without plant hydraulics and groundwater capillary rise (i.e., free drainage); and (c) SoilH, based on CTRL, but uses the CH soil water retention model. All experiments were performed seven loops from 1980 to 2015 (36 years; for a total of 252 years to ensure adequate model spin-up) with NLDAS-2 (Xia et al., 2012) as forcing inputs, and the results of 2001–2015 from the last loop were used in our analysis. We first investigated the impacts of plant and soil hydraulics on average and IAV of annual GPP. We also established linear relationships between the anomalies of the annual GPP and TWSA for observations and modeling results to explore how this relationship would change without proper model representations of plant and soil hydraulics. To be consistent with the GRACE TWSA, the modeled monthly TWSA was derived by subtracting the mean value during 2004–2009 and then summed up to generate the annual TWSA. It should be noted that annual GPP and TWSA were linearly detrended before the following analysis.

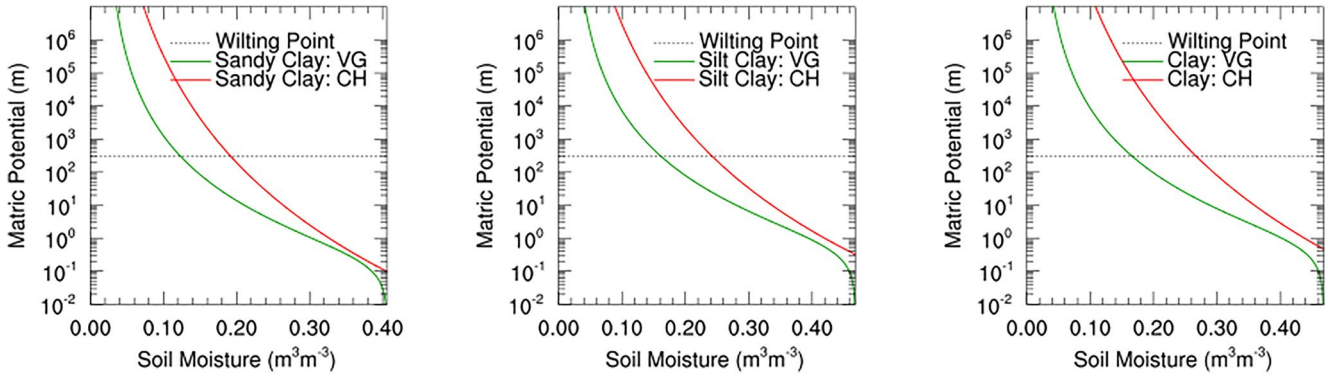

Figure 1. Soil water retention curves of van Genuchten (VG; green lines) and Clapp–Hornberger (CH; red lines) with the wilting point (30 bar, or 306 m; horizontal dashed lines) for sandy clay (39%), silt clay (23%), and clay (20%) in the central US. Percentages in brackets represent fraction of coverage of each soil in the central US (the red box region in Figure 3).

3. Results

3.1. Data Analyses

We first examined the consistency of multiyear mean and normalized IAV (coefficient of variation; CV hereafter) of the linearly detrended GPP among FLUXNET (2001–2011), MODIS (2001–2015), and GOSIF (2001–2015) over the CONUS. We computed the CV value as the ratio of standard deviation to the multiyear mean using linearly detrended data. We removed the long-term trend by linear regression through the whole study. The spatial patterns of multiyear mean and CV of the three products agree well but show substantially different magnitudes (Figure S1 in Supporting Information S1). The multiyear mean of the detrended GPP averaged over the CONUS of GOSIF is the largest (995.4 gC/m^2/year), followed by FLUXNET (866.4 gC/m^2/year) and MODIS (846.2 gC/m^2/year). The averages of the three GPP products for the multiyear mean and CV in the CONUS are 902.6 gC/m^2/year and 0.10, respectively (Figure S2 in Supporting Information S1).

The three GPP products exhibit larger CV values in the central US and the southwest US (Figure S1 in Supporting Information S1) in response to more episodic droughts as reflected by the larger CV of aridity index (Figure S3 in Supporting Information S1). In this study, we focus on the central US for our analyses on the IAVs of the three GPP products and their relationships with the GRACE TWSA. Despite the spread among three GPP products (Figure 2a), the timing and variations agree well (Figure 2b). The CV values of three products in the central US are 0.14, 0.15, and 0.15, respectively, which are higher than those over the CONUS (~0.10). Additionally,

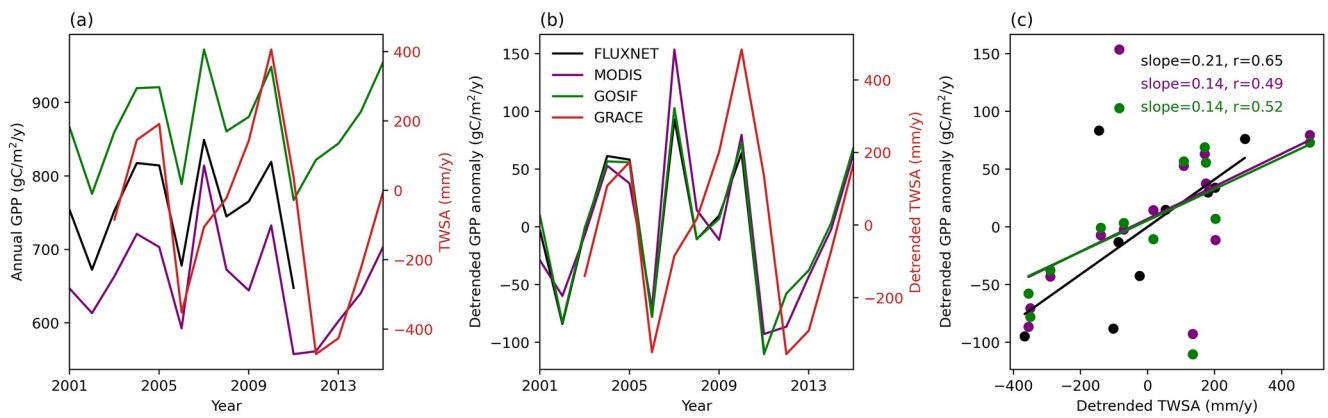

Figure 2. (a) Annual gross primary productivity (GPP; gC/m^2/year) of FLUXNET (2001–2011; black line), MODIS (2001–2015; purple line), and GOSIF (2001–2015; green line) and annual GRACE terrestrial water storage anomaly (TWSA; 2003–2015; mm/year) averaged over the central US (the red box in Figure 3b with a longitude range of 104.0625°W–95.0625°W). (b) The same as (a) but for the detrended anomaly of the GPP products and detrended TWSA. (c) Detrended annual GPP anomaly of the observation-based GPP products versus GRACE TWSA during 2003–2015 (FLUXNET: 2003–2011), with the slopes and Pearson correlation coefficients (r; $p > 0.05$ likely due to the brevity of the GRACE TWSA time series) provided in the panel.

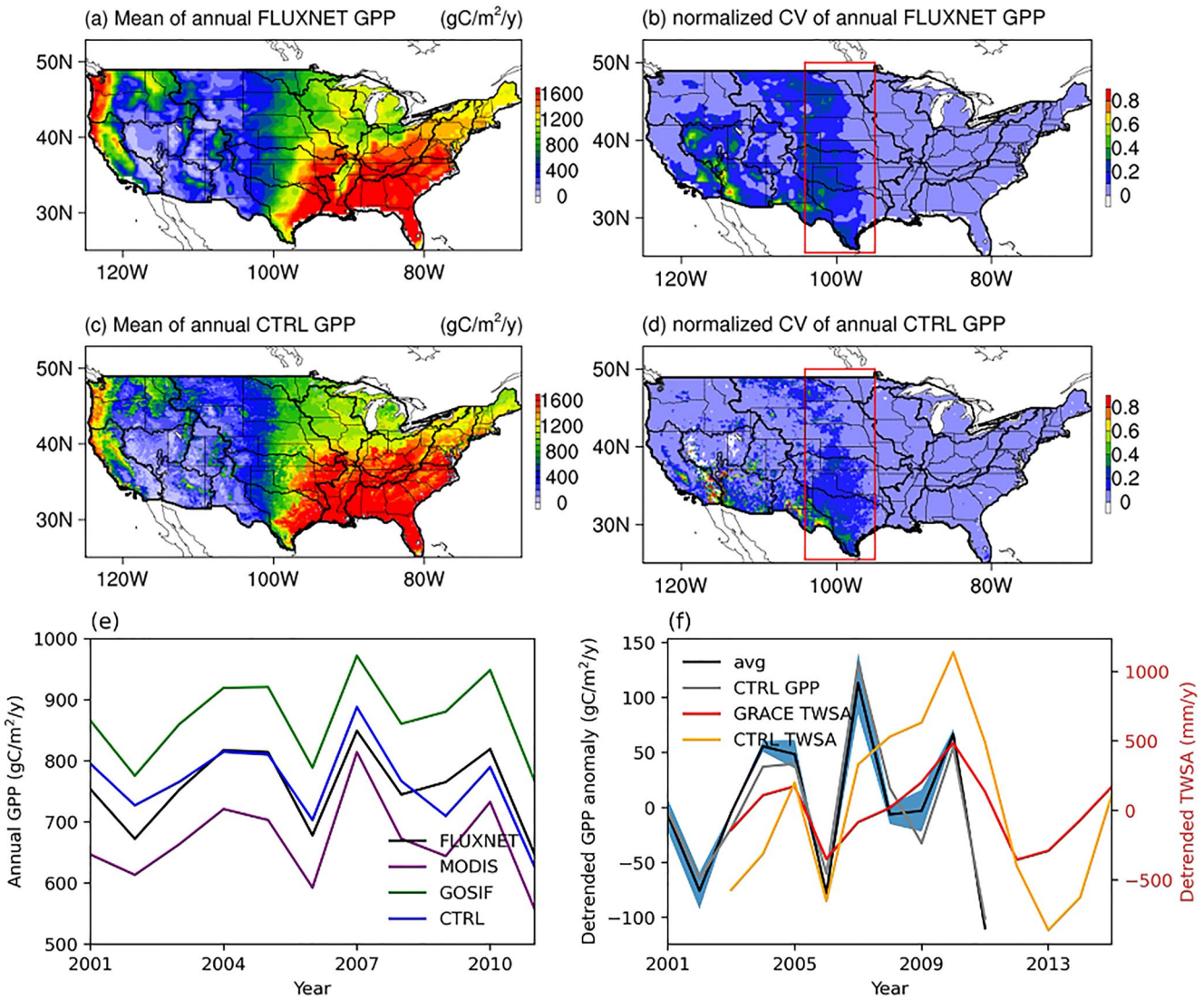

Figure 3. (a) Mean annual gross primary productivity (GPP; gC/m^2/year) and (b) normalized interannual variability (coefficient of variation or CV) of FLUXNET during 2001–2011. (c, d) The same as (a) and (b) but for the CTRL experiment, respectively. Annual GPP was linearly detrended before calculating averages and CVs. (e) Annual GPP of FLUXNET, MODIS, GOSIF, and CTRL for the central US during 2001–2011. (f) Detrended GPP anomaly of CTRL and the average of the detrended anomaly of the three GPP products with ±1 std ("avg" in the legend) during 2001–2011, and detrended TWSA (mm/year) of CTRL and GRACE over the central US during 2003–2015.

the detrended annual GPP anomalies of all the products show a positive correlation with the GRACE TWSA with similar linear regression slopes (or water use efficiency; 0.21, 0.14, and 0.14 gC/mm H_2O for FLUXNET, MODIS, and GOSIF, respectively), despite the insignificant correlation. This insignificance is likely due to the short temporal coverage (2003–2015; Figure 2c), because the detrended anomaly of FLUXNET GPP is significantly correlated to that of a recently reconstructed TWSA in the central US during a longer period from 1982 to 2011 (Figure S4 in Supporting Information S1). It is also possible that the insignificant correlation is caused by the plant and soil hydraulics and/or irrigation. The positive signs indicate that a positive TWSA in wetter years results in an increased plant carbon uptake.

3.2. Model Evaluation

The climatology and CV of the detrended annual GPP during 2001–2015 resulting from CTRL show a similar spatial pattern to those of FLUXNET, MODIS, and GOSIF (Figures 3a–3d and Figure S2 in Supporting

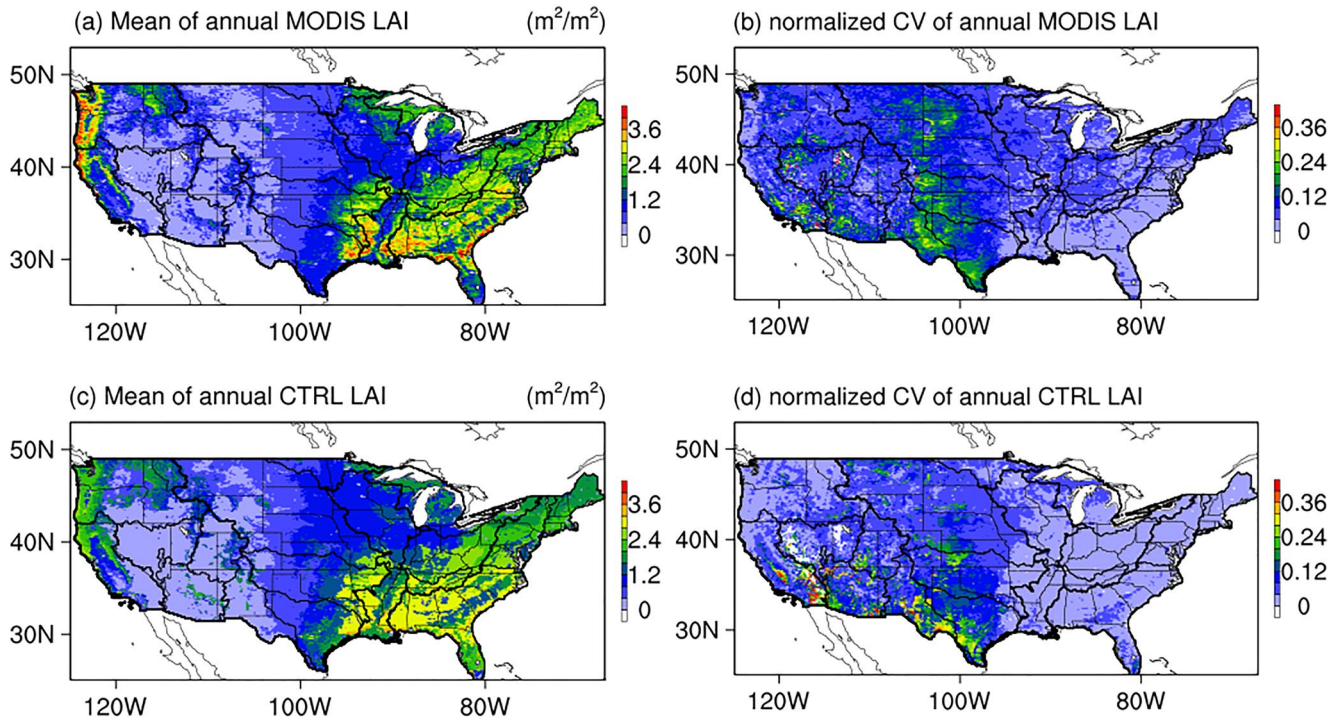

Figure 4. (a) Mean annual leaf area index (LAI; m^2/m^2) and (b) normalized interannual variability (coefficient of variation or CV) of MODIS during 2002–2015. (c, d) The same as (a) and (b) but for the CTRL experiment, respectively. Annual LAI was linearly detrended before calculating averages and CVs.

Information S1) in the CONUS. Both the FLUXNET and simulated GPP by CTRL decreases from over 2,000 gC/m^2/year in the humid southeast US to less than 200 gC/m^2/year in the dry southwest US (Figures 3a and 3c), opposite to that of mean annual aridity index (Figure S3 in Supporting Information S1), suggesting strong hydroclimatic controls (light and water) on ecosystem productivity. The mean annual GPP modeled by CTRL averaged over the CONUS is 875.5 gC/m^2/year, comparable to the average of three observed GPP products (902.6 gC/m^2/year; Figure S2 in Supporting Information S1). The CV value over the CONUS is 0.09, close to the observed (~0.10), and the probability distributions of the annual GPP and CV are comparable to those of the three products (Figure S2 in Supporting Information S1).

Here, we focus on the model performance over the central US because the central US is a dry-to-wet transition zone with more apparent IAVs (the red box in Figure 3b) for both the modeled and observed annual GPP. Due to the large spread of the observed GPP (GOSIF > FLUXNET > MODIS), the simulated GPP falls easily within the range of the observations during 2001–2015 (Figure 3e). The anomaly of the detrended GPP follows closely the observed in terms of timing and amplitude (though slightly overestimated; Figure 3f). The modeled TWSA agrees with GRACE TWSA but the amplitude is overestimated. This may likely result from overestimation of soil surface evaporation especially during droughts (e.g., 2011–2012) due to inadequate process representations (Chang et al., 2018) and/or incomplete search of optimal parameters in the groundwater capillary rise. The simulated GPP–TWSA sensitivity (~0.05 gC/mm H_2O) is lower than the observed water sensitivity (e.g., 0.14 gC/mm H_2O of GOSIF) due to the overestimated amplitude of TWSA. This may be also attributed to uncertainties in modeling the plant intrinsic water use efficiency (Egea et al., 2011) and/or the lower-than-observed ratio of transpiration to ET modeled by Noah-MP (Figure S5 in Supporting Information S1), like most other LSMs (Chang et al., 2018). Both the observed and modeled GPP–TWSA relationships are insignificant ($P > 0.05$) due to the short period of the analysis limited by the observed TWSA availability.

Besides GPP, we also evaluated the modeled LAI and ET against MODIS LAI and PML ET products. Noah-MP well captures spatial distributions of observed LAI in terms of mean annual and IAV during 2002–2015 (Figure 4). Similar to GPP, LAI exhibits high values in the Pacific Northwest and southeastern US with large IAVs in the central US. Modeled ET declines from the southeastern US to the western US, consistent with PML ET (Figure

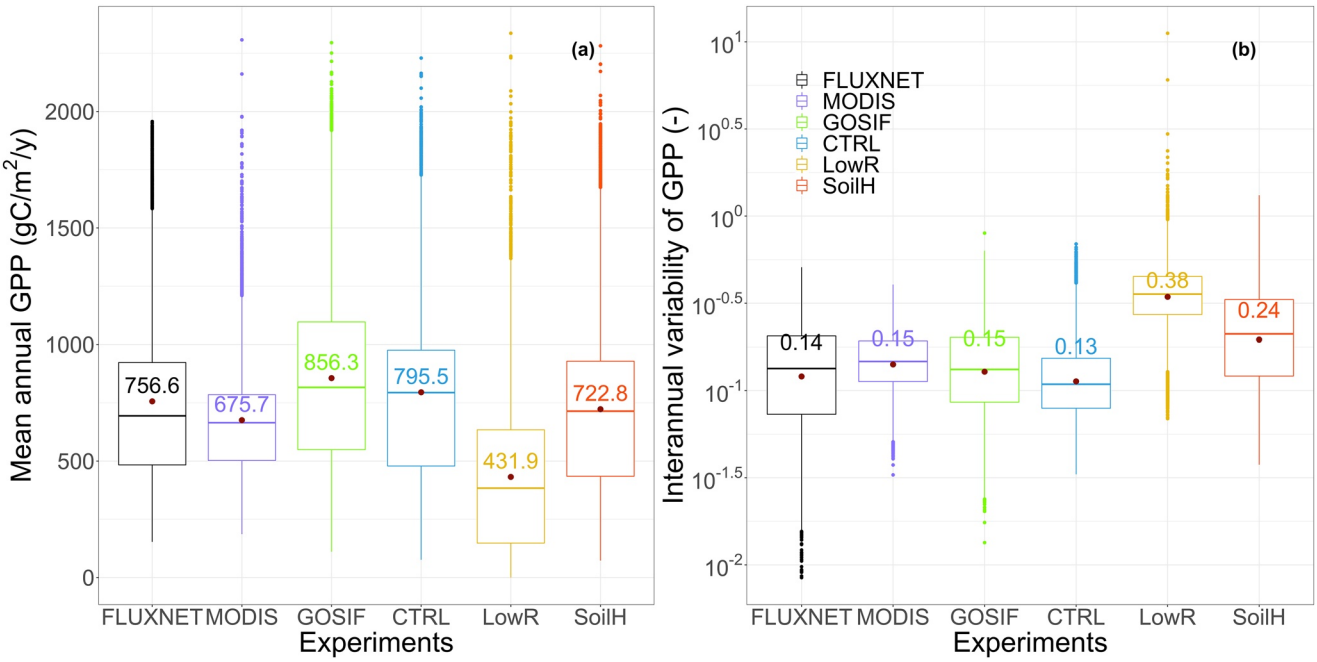

Figure 5. Boxplots of (a) mean annual gross primary productivity (GPP; gC/m^2/year) and (b) the coefficient of variations (CVs) products of FLUXNET (2001–2011; black), MODIS (2001–2015; purple), and GOSIF (2001–2015; green) as well as GPP produced by the models of CTRL (blue), LowR (yellow), and SoilH (red) during 2001–2015 in the central US (the red box in Figure 3). Annual GPP was linearly detrended before calculating averages and CVs.

S6 in Supporting Information S1). In addition, similar spatial patterns between GPP, LAI, and ET indicate strong water and vegetation productivity coupling.

3.3. Key Controls on the IAV of GPP

The mean annual GPP produced by LowR remarkably decreases over almost the entire CONUS but more extensive over the central US (Figures S7a–S7d in Supporting Information S1), reflecting the dominant control of water availability on GPP. The mean annual GPP averaged over the CONUS drops from 875.5 gC/m^2/year by CTRL to 671.1 gC/m^2/year (by 23.3%; Figure S2a in Supporting Information S1). In contrast, the GPP CV is significantly enhanced with the averaged value over the CONUS changing from 0.09 to 0.24 (Figure S2b in Supporting Information S1) due to increased plant water stress (Figures S8a–S8d in Supporting Information S1). The mean annual GPP over the central US is 45.7% lower than that of CTRL, and the GPP IAV is twice higher than that of CTRL (Figure 5). The spatial pattern of GPP decreases (Figure S7b in Supporting Information S1) matches that of aridity variations (Figure S3 in Supporting Information S1). During more frequent and intense droughts in the central US, LowR, without representations of plant hydraulics with dynamic roots and groundwater capillary rise, produces lower GPP (Figure S9 in Supporting Information S1) under enhanced plant water stress, resulting a larger IAV, compared to CTRL.

Compared to CTRL, SoilH slightly reduces the mean and IAV of annual GPP over CONUS (Figures S7e and S7f and Figure S2 in Supporting Information S1) but a substantial reduction of mean annual GPP in the central US by 9.1% to 722.8 from 795.5 gC/m^2/year in CTRL (Figure 5). Also, the CV value averaged over the central US increases from 0.13 to 0.24 (Figure 5b). The CH soil water retention model used in SoilH tends to overestimate soil matric suction than does the VG model, especially in the dry end of the soil water retention curve (Niu et al., 2020). The top three soil types in the central US are sandy clay, silt clay, and clay, accounting for 39%, 23%, and 20% of the central US, respectively. The soil moisture corresponding to the wilting point at 30 bar in SoilH with the CH model are much larger than that in CTRL with the VG model for all these soil types (0.19 vs. 0.12 m^3/m^3 for sandy clay; 0.24 vs. 0.16 m^3/m^3 for silt clay; and 0.27 vs. 0.17 m^3/m^3 for clay; Figure 1). The larger wilting point in soil moisture with the CH model (in SoilH) allows less soil water to be extracted by plant roots

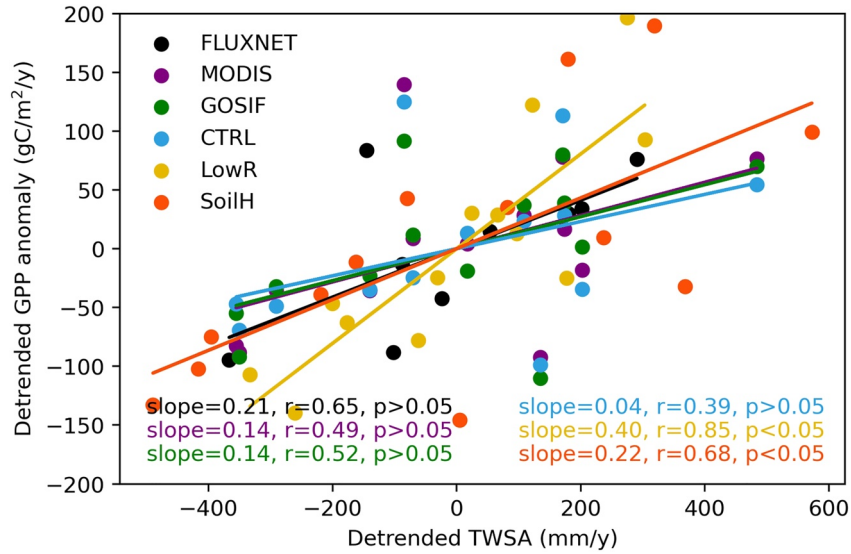

Figure 6. Linear relationships between the detrended annual GPP anomaly (gC/m^2/year) versus terrestrial water storage anomaly (TWSA; mm/year) produced by FLUXNET, MODIS, GOSIF, CTRL, LowR, and SoilH during 2003–2015, except FLUXNET (2003–2011).

for transpiration and photosynthesis, reducing GPP over drought years (Figure S9 in Supporting Information S1) and thus enhancing the GPP IAV.

Over the central US, the correlations between GPP and TWSA are much higher in LowR (0.85) and SoilH (0.68) than in CTRL (0.39; Figure 6) and observation-based data sets (0.49–0.65; Figure 2). Also, the sensitivity of GPP to TWSA is substantially enhanced from 0.04 gC/mm H_2O by CTRL to 0.40 and 0.22 gC/mm H_2O by LowR and SoilH, respectively, both of which are larger than the observed values (0.14–0.21 gC/mm H_2O). The enhanced correlation and sensitivity by LowR and SoilH are mainly caused by the lower RUE resulting from the lower water availability under drought conditions (Figure S10 in Supporting Information S1). This suggests that models without adequate representations of plant and soil hydraulics and surface–groundwater interactions, like LowR and SoilH, may produce lower plant drought resilience and thus overestimate the sensitivity to water availability. However, CTRL with more detailed considerations of these ecohydrological processes produces a weaker sensitivity of GPP to water availability, suggesting that further model developments in ET partitioning and plant intrinsic water use efficiency (Egea et al., 2011) and parameter calibration in these newly added processes (Huo et al., 2019) are needed.

4. Discussion

The model representations of plant and soil hydraulics incorporated in CTRL lead to a better simulation of GPP. More specifically, the model representations in CTRL include augmented descriptions of dynamic root water uptake, plant water storage, carbon biomass allocation into roots, hydrotropic root growth, plant stomatal hydraulic stress, and soil water retention characteristics (Niu et al., 2020). Plant water storage contributes significantly to transpiration by buffering the water stress during daytime through nocturnal water uptake by roots (C. W. Huang et al., 2017) and possibly at seasonal scales in some tropical woodlands (Tian et al., 2018). It also can reduce the risk of xylem embolism as evidenced by observation and modeling experiments (Niu et al., 2020; Vogel et al., 2017; Waring & Running, 1978). The new carbon allocation scheme tends to allocate more GPP to roots under water stress with a maximum of 30% (Niu et al., 2020). Figure 7 shows that CTRL produces a higher root carbon biomass than the other two experiments and thus facilitates root water uptake. In addition, root respiration and growth are regulated by soil temperature and moisture, resulting in a dynamic vertical root distribution. More importantly, the plant stomatal hydraulic stress is parameterized as a function of plant water storage (Niu et al., 2020) to control transpiration and photosynthesis, instead of empirical functions determined by soil water availability (or soil water potential). These empirical functions associate stomatal conductance with soil water conditions, implicitly considering the impacts of vapor pressure deficit and active plant hydraulics on

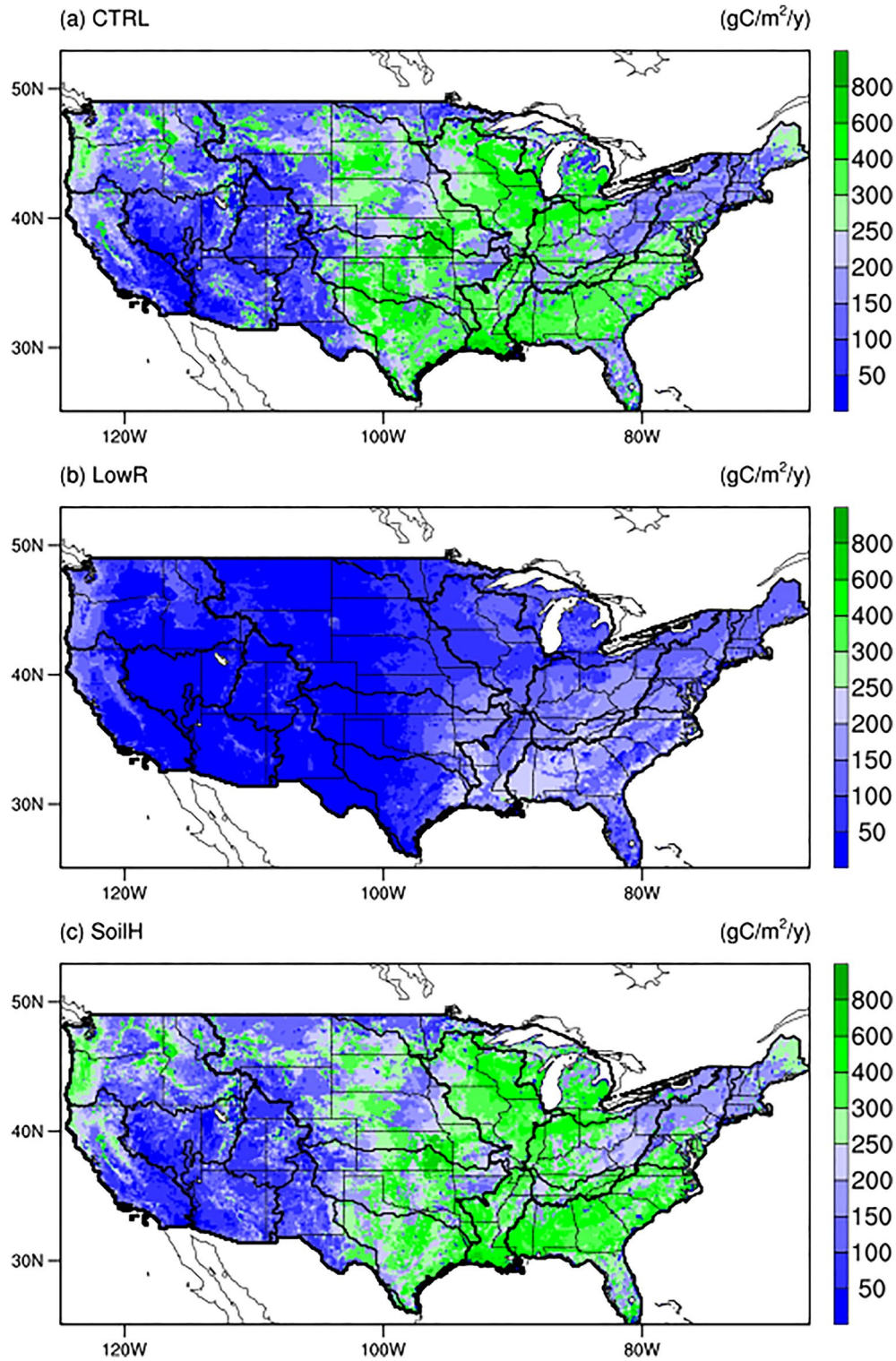

Figure 7. Mean annual root carbon biomass in (a) CTRL, (b) LowR, and (c) SoilH during 2001–2015 (gC/m^2/year).

stomata openings (Kennedy et al., 2019; Sperry & Love, 2015). Trugman et al. (2018) demonstrated remarkable uncertainties in the estimates of terrestrial carbon cycle because photosynthesis processes are regulated by empirical soil moisture (or water potential) functions. These plant hydraulics incorporated together into old models (i.e., the model in LowR) reconcile modeling results with GPP observations. L. Li, Yang, et al. (2021)

implemented a scheme of plant hydraulics into Noah-MP with less attention to root water uptake but more to water transfer through different parts of plants (e.g., stem, root, and leaf) under the assumption of a nonequilibrium hydraulic state between the plant parts. Because the modeled hydraulic effects were tested only at plot scales and tree levels, the model needs further tests, and the model parameters needs further calibrations for various vegetation types before large-scale applications like this study.

The Noah-MP version used in this study also features "HR" (Dawson, 1993; Prieto et al., 2012) through water exchanges between soils and roots. HR facilitates movement of soil water from wetter deep layers to the near-surface drier layers to sustain plant transpiration and soil surface evaporation during dry seasons (i.e., hydraulic lift). On the other hand, HR facilitates soil water infiltration into deep soil layers during rainy periods, which help reduce soil surface evaporation and store more water for the following dry periods (i.e., hydraulic descent). HR is determined by physiological, climatic, and biological factors, such as precipitation amount and spatiotemporal distribution, root–soil water potential gradient, root structure and surface area, accessibility to groundwater, and soil texture (Bleby et al., 2010; Neumann & Cardon, 2012). Previous observation and modeling studies have demonstrated the importance of HR to transpiration over worldwide ecosystems and species, such as in tropical savanna, semiarid grassland, and shrublands (Bleby et al., 2010; Dawson, 1993; Fan et al., 2017; Jackson et al., 2000; J.-E. Lee et al., 2005; Neumann & Cardon, 2012; Wu et al., 2020; Zhou et al., 2020). To assess the impacts of HR on soil evaporation and transpiration, we performed an additional experiment (NoHR), in which HR was turned off by setting up the negative $Q_{R,i}$ values at all layers as 0. Here, we compared ET, transpiration, and soil surface evaporation resulting from NoHR with those from the CTRL experiment (Figure 8). The HR effects are widespread for most of the plants over the modeling domain, because our model assumes that HR occurs when the soil water potential is less than the root water potential at a same layer. In contrast, field experiments suggest that hydraulic lift does not occur until shallow soil water potential drops below a threshold (Meinzer et al., 2004; Neumann & Cardon, 2012) with root architectures spanning horizontal or vertical water potential gradients (Neumann & Cardon, 2012; Scholz et al., 2008). Therefore, Noah-MP tends to overestimate HR, especially with an unconfined aquifer at the soil bottom. The CTRL modeled HR decreases ET by up to ~10% of ET (Figure 8b); CTRL with HR reduces transpiration and increases soil evaporation, more apparently in the western and central US. In other words, the root water is released into the surrounding drier soils, moistening the soil and thus supporting soil surface evaporation. The lower transpiration ratio and plant water use efficiency are unexpected, because a number of observations have shown that HR enhances plant transpiration in the western and central US (Bleby et al., 2010; Hultine et al., 2004; E. Lee et al., 2018; Scott et al., 2008). Further analysis of the modeling results indicates NoHR increases β despite a decrease in the plant water storage (Figure S11 in Supporting Information S1). The increase in β is mainly caused by more reductions in $M_{q,max}$ (Equation 2) that is 3–9 times (dependent on vegetation type) of the water-reserving biomass (dominated by root biomass), which is reduced due to less carbon allocation to roots caused by increases in β ($0.3 \times (1 - \beta)$; see Niu et al., 2020). This unexpected increase in transpiration by NoHR may be resolved by separating the leaf water storage from that for the whole plant.

Despite advanced improvements that are incorporated into our large-scale LSM, belowground plant form and functions and human activities (e.g., irrigation) are still not well represented in our model. First, the improved model prescribed a constant rooting depth of 2 m across spatiotemporal scales. Previous studies reported without enough deep rooting depth, hydraulic lift will be greatly reduced because of lack of access to water sources. Niu et al. (2020) also simulated GPP using the same model as CTRL and reported Noah-MP with three-layer root produces less annual transpiration and GPP with enhanced IAV relative to that with four-layer root. Rooting depth is primarily controlled by topography, groundwater table, and capillary rise (Fan et al., 2017). However, microtopography is still not well represented in ESMs. Swenson et al. (2019) recently incorporated representative hillslopes into the community land model 5.0, reproducing observed upland and lowland ET differences in a catchment. Global-scale hillslope representations are still needed in models given the complex interactions between hillslope, ecosystem, and climate systems. Second, root phenology and mycorrhizal–root interactions were implicitly accounted by calibrating our model against easy-accessible observations, such as GPP, ET, and TWSA, due to lack of large-scale belowground observations. More importantly, some root physiological processes are not incorporated into LSMs, such as root lifespan and mortality (Smithwick et al., 2014). Last, irrigation can minimize the impacts of drought on crop and increase agriculture production. The insignificant correlation between observed GPP and TWSA (Figure 2c) may be a result of irrigation over the High Plains. Neglecting irrigation processes may potentially underestimate the transpiration ratio and GPP but overestimate

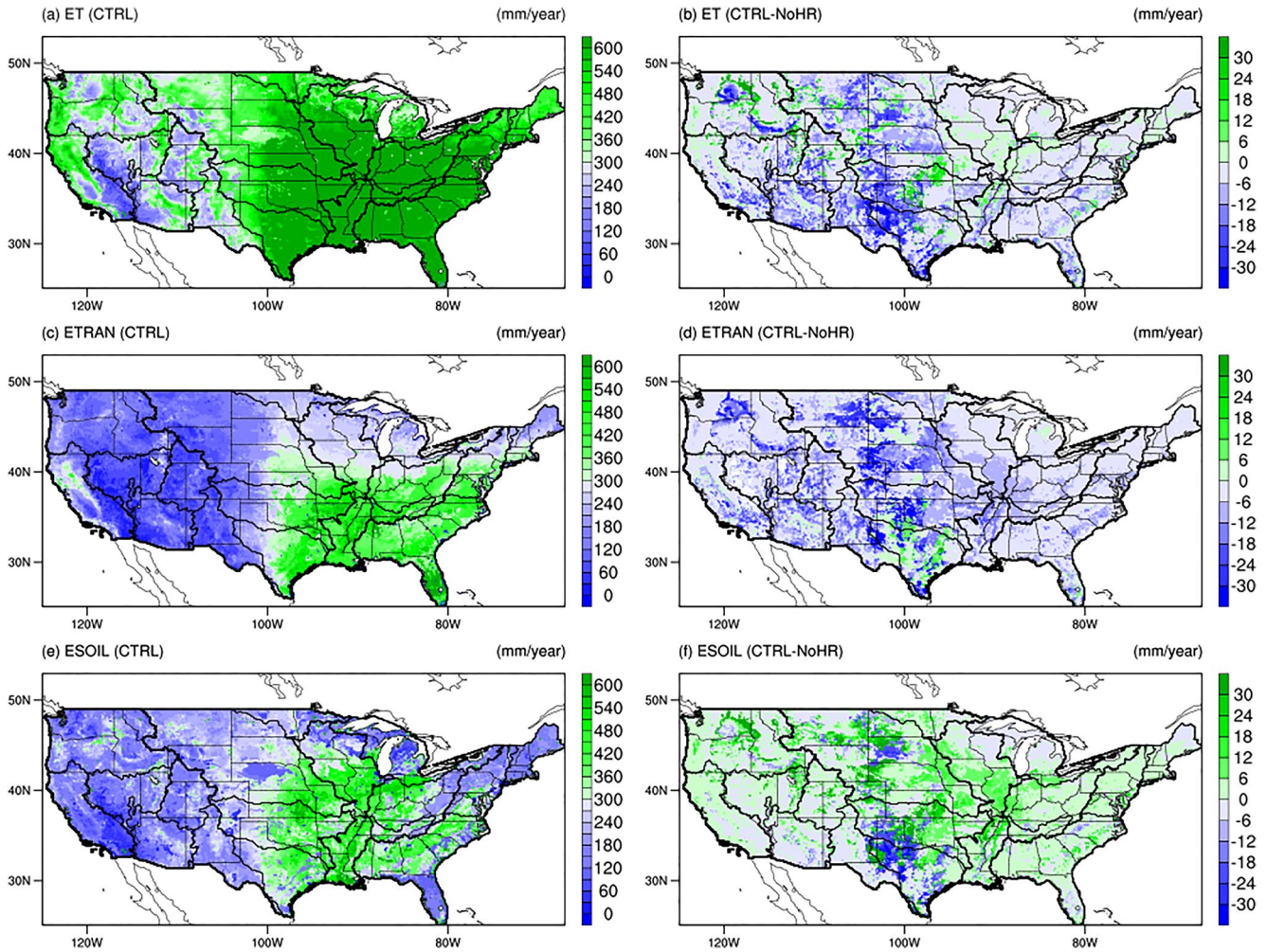

Figure 8. Mean annual (a) evapotranspiration (ET; mm/year), (c) transpiration (ETRAN; mm/year), and (e) soil evaporation (ESOIL; mm/year) of CTRL during 2001–2015. The difference of mean annual (b) evapotranspiration, (d) transpiration, and (f) soil evaporation between CTRL and NoHR during 2001–2015 (mm/year). The NoHR experiment is similar to the CTRL experiment, except with hydraulic redistribution turned off.

GPP IAV and its water sensitivities, which may propagate into climate modeling biases (e.g., precipitation and air temperature) through the land–atmosphere interactions (Dong et al., 2022). The lower-than-observed GPP–TWSA sensitivity resulting from CTRL may be due to the strong groundwater capillary rise effect and/or incomplete search of plant hydraulic parameters. Although recent modeling efforts have been implementing irrigation and other agriculture practice into LSMs (or ESMs), developments of accurate irrigation data considering agricultural management (e.g., amount and timing from local water meters) and climate–agriculture–hydrology interactions at various spatiotemporal scales still need to be further improved (Levis et al., 2012; X. Liu et al., 2016; Z. Zhang et al., 2020). Therefore, concerted large-scale observations and modeling are required to further improve our understandings of belowground biological processes.

5. Conclusion

In this study, we first performed analyses of three GPP products and conducted model experiments to discern the dominant ecohydrological controls on the IAVs of plant carbon uptake as well as their sensitivities to TWSA. We conclude that

1. The various estimates of annual GPP including FLUXNET, MODIS, and GOSIF show more dependence on the water availability over the central US, where more episodic droughts occur than over other regions of the CONUS.

2. Noah-MP with explicit representations of plant and soil hydraulics with the aid of groundwater capillary rise well captures the spatiotemporal variations in GPP with enhanced plant drought resilience and GPP sensitivity to water availability.
3. Noah-MP without plant hydraulics and groundwater capillary rise produces a low plant drought resilience and stronger GPP sensitivity to water availability (e.g., the LowR experiment); so does the CH soil water retention model (the SoilH experiment), which generally produces too strong soil matrix suction (especially under dry conditions), reducing the water availability for plant use.

Models without adequate treatments of plant and soil hydraulics as well as groundwater capillary rise (or lack of irrigation) may substantially overestimate the GPP sensitivity to water availability over regions under episodic droughts. Droughts have become more frequent, intense, and last longer (Trenberth et al., 2014) and will become more widespread under global warming (Dai, 2013; J. Huang et al., 2016). Terrestrial ecosystems may likely experience intensified variations in hydroclimatic conditions, enhancing the IAV of plant carbon uptake. However, current LSMs or ecosystem models may overestimate the IAV of GPP and the water sensitivity of GPP due mainly to the low plant drought resilience resulting from inadequate representations of some key ecohydrological processes.

This study highlights the importance of improved representations of ecohydrological processes, for example, plant and soil hydraulics and surface–groundwater interactions in ESMs. We strongly suggest the use of the VG hydraulic model to replace the most commonly used CH model in land surface modeling, which produces too strong soil suction of water especially in dry conditions.

Data Availability Statement

The data used in this study are available online: NLDAS-2 forcing data (http://www.emc.ncep.noaa.gov/mmb/nldas/); the 1-km hybrid State Soil Geographic Database and the USGS 24-category vegetation data (https://ral.ucar.edu/solutions/products/noah-multiparameterization-land-surface-model-noah-mp-lsm); the FLUXNET-MTE GPP (https://www.bgc-jena.mpg.de/geodb/projects/Home.php); the MODIS GPP (http://files.ntsg.umt.edu/data/NTSG_Products/MOD17/GeoTIFF/MOD17A2/); the MODIS LAI (http://globalchange.bnu.edu.cn/research/laiv6#download); the SIF-based GPP (https://globalecology.unh.edu); the GRACE TWSA data (http://grace.jpl.nasa.gov); the reconstructed GRACE TWSA data (https://doi.org/10.5061/dryad.z612jm6bt); and the PML ET products (https://data.csiro.au/collections/collection/CIcsiro:17375v2).

Acknowledgments
This study was supported by the NASA MAP Program (80NSSC17K0352), NOAA Award (NA20OAR4310337), and DOE Earth System Modeling Program (DE-AC52-498657 07NA27344/B639244). We thank the editorial team and three anonymous reviewers for the insightful comments that greatly improved the quality of this work.

References

Ahlström, A., Raupach, M. R., Schurgers, G., Smith, B., Arneth, A., Jung, M., et al. (2015). The dominant role of semi-arid ecosystems in the trend and variability of the land CO_2 sink. *Science*, *348*(6237), 895–899. https://doi.org/10.1126/science.aaa1668

Arora, V. K., Katavouta, A., Williams, R. G., Jones, C. D., Brovkin, V., Friedlingstein, P., et al. (2020). Carbon–concentration and carbon–climate feedbacks in CMIP6 models and their comparison to CMIP5 models. *Biogeosciences*, *17*(16), 4173–4222. https://doi.org/10.5194/bg-17-4173-2020

Beven, K., & Germann, P. (1982). Macropores and water flow in soils. *Water Resources Research*, *18*(5), 1311–1325. https://doi.org/10.1029/WR018i005p01311

Biederman, J. A., Scott, R. L., Bell, T. W., Bowling, D. R., Dore, S., Garatuza-Payan, J., et al. (2017). CO_2 exchange and evapotranspiration across dryland ecosystems of southwestern North America. *Global Change Biology*, *23*(10), 4204–4221. https://doi.org/10.1111/gcb.13686

Bleby, T. M., Mcelrone, A. J., & Jackson, R. B. (2010). Water uptake and hydraulic redistribution across large woody root systems to 20 m depth. *Plant, Cell and Environment*, *33*(12), 2132–2148. https://doi.org/10.1111/j.1365-3040.2010.02212.x

Bonan, G. B. (1996). *Land surface model (LSM version 1.0) for ecological, hydrological, and atmospheric studies: Technical description and users guide (Technical note)*. Boulder, CO: National Center for Atmospheric Research.

Bousquet, P., Peylin, P., Ciais, P., Le Quéré, C., Friedlingstein, P., & Tans, P. P. (2000). Regional changes in carbon dioxide fluxes of land and oceans since 1980. *Science*, *290*(5495), 1342–1346. https://doi.org/10.1126/science.290.5495.1342

Brooks, R. H., & Corey, A. T. (1964). Hydraulic properties of porous media and their relation to drainage design. *Transactions of the ASAE*, *7*(1), 26–0028. https://doi.org/10.13031/2013.40684

Chang, L. L., Dwivedi, R., Knowles, J. F., Fang, Y. H., Niu, G. Y., Pelletier, J. D., et al. (2018). Why do large-scale land surface models produce a low ratio of transpiration to evapotranspiration? *Journal of Geophysical Research: Atmospheres*, *123*, 9109–9130. https://doi.org/10.1029/2018JD029159

Clapp, R. B., & Hornberger, G. M. (1978). Empirical equations for some soil hydraulic properties. *Water Resources Research*, *14*(4), 601–604. https://doi.org/10.1029/WR014i004p00601

Cox, P. M., Pearson, D., Booth, B. B., Friedlingstein, P., Huntingford, C., Jones, C. D., & Luke, C. M. (2013). Sensitivity of tropical carbon to climate change constrained by carbon dioxide variability. *Nature*, *494*(7437), 341–344. https://doi.org/10.1038/nature11882

Dai, A. (2013). Increasing drought under global warming in observations and models. *Nature Climate Change*, *3*(1), 52–58. https://doi.org/10.1038/nclimate1633

Dawson, T. E. (1993). Hydraulic lift and water use by plants: Implications for water balance, performance and plant–plant interactions. *Oecologia*, *95*(4), 565–574. https://doi.org/10.1007/BF00317442

Dickinson, R. E., Shaikh, M., Bryant, R., & Graumlich, L. (1998). Interactive canopies for a climate model. *Journal of Climate*, *11*(11), 2823–2836. https://doi.org/10.1175/1520-0442(1998)011<2823:ICFACM>2.0.CO;2;2

Dong, J., Lei, F., & Crow, W. T. (2022). Land transpiration–evaporation partitioning errors responsible for modeled summertime warm bias in the central United States. *Nature Communications*, *13*(1), 1–8. https://doi.org/10.1038/s41467-021-27938-6

Egea, G., Verhoef, A., & Vidale, P. L. (2011). Towards an improved and more flexible representation of water stress in coupled photosynthesis–stomatal conductance models. *Agricultural and Forest Meteorology*, *151*(10), 1370–1384. https://doi.org/10.1016/j.agrformet.2011.05.019

Fan, Y., Miguez-Macho, G., Jobbágy, E. G., Jackson, R. B., & Otero-Casal, C. (2017). Hydrologic regulation of plant rooting depth. *Proceedings of the National Academy of Sciences of the United States of America*, *114*(40), 10572–10577. https://doi.org/10.1073/pnas.1712381114

Friedlingstein, P., Cox, P., Betts, R., Bopp, L., von Bloh, W., Brovkin, V., et al. (2006). Climate–carbon cycle feedback analysis: Results from the C4MIP model intercomparison. *Journal of Climate*, *19*(14), 3337–3353. https://doi.org/10.1175/JCLI3800.1

Green, J. K., Seneviratne, S. I., Berg, A. M., Findell, K. L., Hagemann, S., Lawrence, D. M., & Gentine, P. (2019). Large influence of soil moisture on long-term terrestrial carbon uptake. *Nature*, *565*(7740), 476–479. https://doi.org/10.1038/s41586-018-0848-x

Gulden, L. E., Rosero, E., Yang, Z. L., Rodell, M., Jackson, C. S., Niu, G. Y., et al. (2007). Improving land-surface model hydrology: Is an explicit aquifer model better than a deeper soil profile? *Geophysical Research Letters*, *34*, L09402. https://doi.org/10.1029/2007GL029804

Huang, C. W., Domec, J. C., Ward, E. J., Duman, T., Manoli, G., Parolari, A. J., & Katul, G. G. (2017). The effect of plant water storage on water fluxes within the coupled soil–plant system. *New Phytologist*, *213*(3), 1093–1106. https://doi.org/10.1111/nph.14273

Huang, J., Yu, H., Guan, X., Wang, G., & Guo, R. (2016). Accelerated dryland expansion under climate change. *Nature Climate Change*, *6*(2), 166–171. https://doi.org/10.1038/nclimate2837

Hultine, K. R., Scott, R., Cable, W., Goodrich, D., & Williams, D. (2004). Hydraulic redistribution by a dominant, warm-desert phreatophyte: Seasonal patterns and response to precipitation pulses. *Functional Ecology*, *18*(4), 530–538. https://doi.org/10.1111/j.0269-8463.2004.00867.x

Humphrey, V., Berg, A., Ciais, P., Gentine, P., Jung, M., Reichstein, M., et al. (2021). Soil moisture–atmosphere feedback dominates land carbon uptake variability. *Nature*, *592*(7852), 65–69. https://doi.org/10.1038/s41586-021-03325-5

Humphrey, V., Zscheischler, J., Ciais, P., Gudmundsson, L., Sitch, S., & Seneviratne, S. I. (2018). Sensitivity of atmospheric CO_2 growth rate to observed changes in terrestrial water storage. *Nature*, *560*(7720), 628–631. https://doi.org/10.1038/s41586-018-0424-4

Huo, X., Gupta, H., Niu, G. Y., Gong, W., & Duan, Q. (2019). Parameter sensitivity analysis for computationally intensive spatially distributed dynamical environmental systems models. *Journal of Advances in Modeling Earth Systems*, *11*, 2896–2909. https://doi.org/10.1029/2018MS001573

Jackson, R. B., Schenk, H., Jobbagy, E., Canadell, J., Colello, G., Dickinson, R., et al. (2000). Belowground consequences of vegetation change and their treatment in models. *Ecological Applications*, *10*(2), 470–483. https://doi.org/10.1890/1051-0761(2000)010[0470:BCOVCA]2.0.CO;2

Jung, M., Reichstein, M., Margolis, H. A., Cescatti, A., Richardson, A. D., Arain, M. A., et al. (2011). Global patterns of land–atmosphere fluxes of carbon dioxide, latent heat, and sensible heat derived from eddy covariance, satellite, and meteorological observations. *Journal of Geophysical Research*, *116*, G00J07. https://doi.org/10.1029/2010JG001566

Jung, M., Reichstein, M., Schwalm, C. R., Huntingford, C., Sitch, S., Ahlström, A., et al. (2017). Compensatory water effects link yearly global land CO_2 sink changes to temperature. *Nature*, *541*(7638), 516–520. https://doi.org/10.1038/nature20780

Kennedy, D., Swenson, S., Oleson, K. W., Lawrence, D. M., Fisher, R., Lola da Costa, A. C., & Gentine, P. (2019). Implementing plant hydraulics in the community land model, version 5. *Journal of Advances in Modeling Earth Systems*, *11*, 485–513. https://doi.org/10.1029/2018MS001500

Koster, R. D., Dirmeyer, P. A., Guo, Z., Bonan, G., Chan, E., Cox, P., et al. (2004). Regions of strong coupling between soil moisture and precipitation. *Science*, *305*(5687), 1138–1140. https://doi.org/10.1126/science.1100217

Landerer, F. W., & Swenson, S. (2012). Accuracy of scaled GRACE terrestrial water storage estimates. *Water Resources Research*, *48*, W04531. https://doi.org/10.1029/2011WR011453

Lee, E., Kumar, P., Barron-Gafford, G. A., Hendryx, S. M., Sanchez-Cañete, E. P., Minor, R. L., et al. (2018). Impact of hydraulic redistribution on multispecies vegetation water use in a semiarid savanna ecosystem: An experimental and modeling synthesis. *Water Resources Research*, *54*, 4009–4027. https://doi.org/10.1029/2017WR021006

Lee, J.-E., Oliveira, R. S., Dawson, T. E., & Fung, I. (2005). Root functioning modifies seasonal climate. *Proceedings of the National Academy of Sciences of the United States of America*, *102*(49), 17576–17581. https://doi.org/10.1073/pnas.0508785102

Levis, S., Bonan, G. B., Kluzek, E., Thornton, P. E., Jones, A., Sacks, W. J., & Kucharik, C. J. (2012). Interactive crop management in the Community Earth System Model (CESM1): Seasonal influences on land–atmosphere fluxes. *Journal of Climate*, *25*(14), 4839–4859. https://doi.org/10.1175/JCLI-D-11-00446.1

Li, F., Kusche, J., Chao, N., Wang, Z., & Löcher, A. (2021). Long-term (1979–present) total water storage anomalies over the global land derived by reconstructing GRACE data. *Geophysical Research Letters*, *48*, e2021GL093492. https://doi.org/10.1029/2021GL093492

Li, L., Yang, Z. L., Matheny, A. M., Zheng, H., Swenson, S. C., Lawrence, D. M., et al. (2021). Representation of plant hydraulics in the Noah-MP land surface model: Model development and multiscale evaluation. *Journal of Advances in Modeling Earth Systems*, *13*, e2020MS002214. https://doi.org/10.1029/2020MS002214

Li, X., & Xiao, J. (2019a). A global, 0.05-degree product of solar-induced chlorophyll fluorescence derived from OCO-2, MODIS, and reanalysis data. *Remote Sensing*, *11*(5), 517. https://doi.org/10.3390/rs11050517

Li, X., & Xiao, J. (2019b). Mapping photosynthesis solely from solar-induced chlorophyll fluorescence: A global, fine-resolution dataset of gross primary production derived from OCO-2. *Remote Sensing*, *11*(21), 2563. https://doi.org/10.3390/rs11212563

Lin, Y.-S., Medlyn, B. E., Duursma, R. A., Prentice, I. C., Wang, H., Baig, S., et al. (2015). Optimal stomatal behaviour around the world. *Nature Climate Change*, *5*(5), 459–464. https://doi.org/10.1038/nclimate2550

Liu, X., Chen, F., Barlage, M., Zhou, G., & Niyogi, D. (2016). Noah-MP-Crop: Introducing dynamic crop growth in the Noah-MP land surface model. *Journal of Geophysical Research: Atmospheres*, *121*, 13953–13972. https://doi.org/10.1002/2016JD025597

Liu, Y., Kumar, M., Katul, G. G., Feng, X., & Konings, A. G. (2020). Plant hydraulics accentuates the effect of atmospheric moisture stress on transpiration. *Nature Climate Change*, *10*(7), 691–695. https://doi.org/10.1038/s41558-020-0781-5

Loustau, D., Domec, J.-C., & Bosc, A. (1998). Interpreting the variations in xylem sap flux density within the trunk of maritime pine (*Pinus pinaster* Ait.): Application of a model for calculating water flows at tree and stand levels. *Annales des Sciences Forestieres*, *55*(1–2), 29–46. https://doi.org/10.1051/forest:19980103

Ma, N., Niu, G. Y., Xia, Y., Cai, X., Zhang, Y., Ma, Y., & Fang, Y. (2017). A systematic evaluation of Noah-MP in simulating land–atmosphere energy, water, and carbon exchanges over the continental United States. *Journal of Geophysical Research: Atmospheres*, *122*, 12245–12268. https://doi.org/10.1002/2017JD027597

Meinzer, F., Brooks, J., Bucci, S., Goldstein, G., Scholz, F., & Warren, J. (2004). Converging patterns of uptake and hydraulic redistribution of soil water in contrasting woody vegetation types. *Tree Physiology*, *24*(8), 919–928. https://doi.org/10.1093/treephys/24.8.919

Neumann, R. B., & Cardon, Z. G. (2012). The magnitude of hydraulic redistribution by plant roots: A review and synthesis of empirical and modeling studies. *New Phytologist*, *194*(2), 337–352. https://doi.org/10.1111/j.1469-8137.2012.04088.x

Niu, G. Y., Fang, Y. H., Chang, L. L., Jin, J., Yuan, H., & Zeng, X. (2020). Enhancing the Noah-MP ecosystem response to droughts with an explicit representation of plant water storage supplied by dynamic root water uptake. *Journal of Advances in Modeling Earth Systems*, *12*, e2020MS002062. https://doi.org/10.1029/2020MS002062

Niu, G. Y., Yang, Z. L., Dickinson, R. E., Gulden, L. E., & Su, H. (2007). Development of a simple groundwater model for use in climate models and evaluation with Gravity Recovery and Climate Experiment data. *Journal of Geophysical Research*, *112*, D07103. https://doi.org/10.1029/2006JD007522

Niu, G. Y., Yang, Z. L., Mitchell, K. E., Chen, F., Ek, M. B., Barlage, M., et al. (2011). The community Noah land surface model with multiparameterization options (Noah-MP): 1. Model description and evaluation with local-scale measurements. *Journal of Geophysical Research*, *116*, D12109. https://doi.org/10.1029/2010JD015139

Poulter, B., Frank, D., Ciais, P., Myneni, R. B., Andela, N., Bi, J., et al. (2014). Contribution of semi-arid ecosystems to interannual variability of the global carbon cycle. *Nature*, *509*(7502), 600–603. https://doi.org/10.1038/nature13376

Prieto, I., Armas, C., & Pugnaire, F. I. (2012). Water release through plant roots: New insights into its consequences at the plant and ecosystem level. *New Phytologist*, *193*(4), 830–841. https://doi.org/10.1111/j.1469-8137.2011.04039.x

Quéré, C. L., Andrew, R. M., Friedlingstein, P., Sitch, S., Pongratz, J., Manning, A. C., et al. (2018). Global carbon budget 2017. *Earth System Science Data*, *10*(1), 405–448. https://doi.org/10.5194/essd-10-405-2018

Roderick, M. L., & Canny, M. J. (2005). A mechanical interpretation of pressure chamber measurements—What does the strength of the squeeze tell us? *Plant Physiology and Biochemistry*, *43*(4), 323–336. https://doi.org/10.1016/j.plaphy.2005.02.014

Sakumura, C., Bettadpur, S., & Bruinsma, S. (2014). Ensemble prediction and intercomparison analysis of GRACE time-variable gravity field models. *Geophysical Research Letters*, *41*, 1389–1397. https://doi.org/10.1002/2013GL058632

Scholz, F., Bucci, S., Goldstein, G., Moreira, M., Meinzer, F., Domec, J.-C., et al. (2008). Biophysical and life-history determinants of hydraulic lift in Neotropical savanna trees. *Functional Ecology*, *22*(5), 773–786. https://doi.org/10.1111/j.1365-2435.2008.01452.x

Scott, R. L., Cable, W. L., & Hultine, K. R. (2008). The ecohydrologic significance of hydraulic redistribution in a semiarid savanna. *Water Resources Research*, *44*, W02440. https://doi.org/10.1029/2007WR006149

Smithwick, E. A., Lucash, M. S., McCormack, M. L., & Sivandran, G. (2014). Improving the representation of roots in terrestrial models. *Ecological Modelling*, *291*, 193–204. https://doi.org/10.1016/j.ecolmodel.2014.07.023

Sperry, J. S., & Love, D. M. (2015). What plant hydraulics can tell us about responses to climate-change droughts. *New Phytologist*, *207*(1), 14–27. https://doi.org/10.1111/nph.13354

Sun, Y., Wang, C., Chen, H. Y., & Ruan, H. (2020). Response of plants to water stress: A meta-analysis. *Frontiers of Plant Science*, *11*, 978. https://doi.org/10.3389/fpls.2020.00978

Swenson, S. C., Clark, M., Fan, Y., Lawrence, D. M., & Perket, J. (2019). Representing intrahillslope lateral subsurface flow in the community land model. *Journal of Advances in Modeling Earth Systems*, *11*, 4044–4065. https://doi.org/10.1029/2019MS001833

Tian, F., Wigneron, J.-P., Ciais, P., Chave, J., Ogée, J., Peñuelas, J., et al. (2018). Coupling of ecosystem-scale plant water storage and leaf phenology observed by satellite. *Nature Ecology & Evolution*, *2*(9), 1428–1435. https://doi.org/10.1038/s41559-018-0630-3

Trenberth, K. E., Dai, A., Van Der Schrier, G., Jones, P. D., Barichivich, J., Briffa, K. R., & Sheffield, J. (2014). Global warming and changes in drought. *Nature Climate Change*, *4*(1), 17–22. https://doi.org/10.1038/nclimate2067

Trugman, A., Medvigy, D., Mankin, J., & Anderegg, W. (2018). Soil moisture stress as a major driver of carbon cycle uncertainty. *Geophysical Research Letters*, *45*, 6495–6503. https://doi.org/10.1029/2018GL078131

Van Genuchten, M. T. (1980). A closed-form equation for predicting the hydraulic conductivity of unsaturated soils. *Soil Science Society of America Journal*, *44*(5), 892–898. https://doi.org/10.2136/sssaj1980.03615995004400050002x

Vogel, T., Votrubova, J., Dohnal, M., & Dusek, J. (2017). A simple representation of plant water storage effects in coupled soil water flow and transpiration stream modeling. *Vadose Zone Journal*, *16*(5), 1–10. https://doi.org/10.2136/vzj2016.12.0128

Wang, P., Niu, G. Y., Fang, Y. H., Wu, R. J., Yu, J. J., Yuan, G. F., et al. (2018). Implementing dynamic root optimization in Noah-MP for simulating phreatophytic root water uptake. *Water Resources Research*, *54*, 1560–1575. https://doi.org/10.1002/2017WR021061

Waring, R. H., & Running, S. W. (1978). Sapwood water storage: Its contribution to transpiration and effect upon water conductance through the stems of old-growth Douglas-fir. *Plant, Cell and Environment*, *1*(2), 131–140. https://doi.org/10.1111/j.1365-3040.1978.tb00754.x

Wolf, S., Keenan, T. F., Fisher, J. B., Baldocchi, D. D., Desai, A. R., Richardson, A. D., et al. (2016). Warm spring reduced carbon cycle impact of the 2012 US summer drought. *Proceedings of the National Academy of Sciences of the United States of America*, *113*(21), 5880–5885. https://doi.org/10.1073/pnas.1519620113

Wu, H., Fu, C., Wu, H., & Zhang, L. (2020). Plant hydraulic stress strategy improves model predictions of the response of gross primary productivity to drought across China. *Journal of Geophysical Research: Atmospheres*, *125*, e2020JD033476. https://doi.org/10.1029/2020JD033476

Xia, Y., Mitchell, K., Ek, M., Cosgrove, B., Sheffield, J., Luo, L., et al. (2012). Continental-scale water and energy flux analysis and validation for North American Land Data Assimilation System project phase 2 (NLDAS-2): 2. Validation of model-simulated streamflow. *Journal of Geophysical Research*, *117*, D03110. https://doi.org/10.1029/2011JD016051

Yang, Z. L., Niu, G. Y., Mitchell, K. E., Chen, F., Ek, M. B., Barlage, M., et al. (2011). The community Noah land surface model with multiparameterization options (Noah-MP): 2. Evaluation over global river basins. *Journal of Geophysical Research*, *116*, D12110. https://doi.org/10.1029/2010JD015140

Yuan, H., Dai, Y., Xiao, Z., Ji, D., & Shangguan, W. (2011). Reprocessing the MODIS leaf area index products for land surface and climate modelling. *Remote Sensing of Environment*, *115*(5), 1171–1187. https://doi.org/10.1016/j.rse.2011.01.001

Zhang, Y., Peña-Arancibia, J. L., McVicar, T. R., Chiew, F. H., Vaze, J., Liu, C., et al. (2016). Multi-decadal trends in global terrestrial evapotranspiration and its components. *Scientific Reports*, *6*(1), 1–12. https://doi.org/10.1038/srep19124

Zhang, Z., Barlage, M., Chen, F., Li, Y., Helgason, W., Xu, X., et al. (2020). Joint modeling of crop and irrigation in the central United States using the Noah-MP land surface model. *Journal of Advances in Modeling Earth Systems*, *12*, e2020MS002159. https://doi.org/10.1029/2020MS002159

Zhao, M., Heinsch, F. A., Nemani, R. R., & Running, S. W. (2005). Improvements of the MODIS terrestrial gross and net primary production global data set. *Remote Sensing of Environment*, *95*(2), 164–176. https://doi.org/10.1016/j.rse.2004.12.011

Zhao, M., & Running, S. W. (2010). Drought-induced reduction in global terrestrial net primary production from 2000 through 2009. *Science*, *329*(5994), 940–943. https://doi.org/10.1126/science.1192666

Zhao, M., Running, S. W., & Nemani, R. R. (2006). Sensitivity of Moderate Resolution Imaging Spectroradiometer (MODIS) terrestrial primary production to the accuracy of meteorological reanalyses. *Journal of Geophysical Research*, *111*, G01002. https://doi.org/10.1029/2004JG000004

Zhou, Y., Wigley, B. J., Case, M. F., Coetsee, C., & Staver, A. C. (2020). Rooting depth as a key woody functional trait in savannas. *New Phytologist*, *227*(5), 1350–1361. https://doi.org/10.1111/nph.16613

Zhu, Q., Riley, W. J., Tang, J., Collier, N., Hoffman, F. M., Yang, X., & Bisht, G. (2019). Representing nitrogen, phosphorus, and carbon interactions in the E3SM land model: Development and global benchmarking. *Journal of Advances in Modeling Earth Systems*, *11*, 2238–2258. https://doi.org/10.1029/2018MS001571